

Rational Approaches for the Design of Effective Human Immunodeficiency Virus Type 1 Nonnucleoside Reverse Transcriptase Inhibitors

Sergio R. Ribone,[†] Mario A. Quevedo,[†] Marcela Madrid,^{*,†} and Margarita C. Briñón^{*,‡}

Departamento de Farmacia, Facultad de Ciencias Químicas, Ciudad Universitaria, Universidad Nacional de Córdoba, X5000HUA, Córdoba, Argentina, and Pittsburgh Supercomputing Center, Pittsburgh, Pennsylvania 15213, United States

Received April 29, 2010

The binding of several classes of nonnucleoside reverse transcriptase inhibitors (NNRTIs) to wild-type (wtRT) and K103N mutant (mRT) human immunodeficiency virus type 1 (HIV-1) reverse transcriptase is studied by molecular dynamics and energy decomposition techniques. The imidoylthiourea (ITU), diaryltriazine (DATA), and diarylpurimidine (DAPY) NNRTIs studied maintain the hydrogen bond with Lys101 during the 3 ns molecular dynamics trajectories. When bound to mRT, all the DAPYs studied establish hydrogen bonds with Glu138; among these, those of the potent inhibitors TMC120 and TMC125 are water-mediated. The molecular interactions of the NNRTIs in the binding pocket are correlated to the drugs' potency. Quantitative free energy analyses show a linear relationship between the van der Waals energetic component and the potency against wtRT. The molecular basis of the interaction between NNRTIs and RT presented here provide quantitative approaches for the design of novel effective anti-HIV drugs.

INTRODUCTION

The reverse transcriptase (RT) of the human immunodeficiency virus type 1 (HIV-1) is an enzyme essential for the replication of the virus, being responsible for the reverse transcription of viral RNA into cDNA.^{1–3} RT is one of the main therapeutic targets for anti-HIV drugs used in the treatment of acquired immunodeficiency syndrome (AIDS).^{1,4} Among RT inhibitors, the nonnucleoside reverse transcriptase inhibitors (NNRTIs) elicit RT inhibition by binding to an allosteric pocket located 10 Å away from the DNA polymerase active site, identified as the nonnucleoside inhibitors binding pocket (NNIBP).^{2,3,5} Unfortunately, NNRTI potency is dramatically reduced by the emergence of viral strains containing mutated RT.^{2,5,6} Thus, the development of novel chemical entities with high affinity for the mutated NNIBP has been a very active research field in recent years.

The internal surface of NNIBP is predominantly hydrophobic and is formed mostly by residues from the p66 subunit, including aromatic (Tyr181, Tyr188, Phe227, and Trp229) and aliphatic (Pro95, Leu100, Val106, Val179, Leu234, and Pro236) hydrophobic amino acid residues, and by Glu138 of the p51 subunit.^{2,5,7,8} In general, NNRTIs establish extensive hydrophobic interactions with NNIBP residues, including van der Waals and $\pi-\pi$ stacking interactions with aromatic amino acid side chains, and form hydrogen bonds with the backbones of hydrophilic residues, such as Lys101 and Lys103.^{2,5,7,8} The most common mutations conferring resistance in NNRTI-treated patients include K103N, K101E, L100I, V106A, Y181C, Y188L, and G190A, occurring alone or in combinations. On the basis of

available experimental data, it has been suggested that mutations cause drug resistance by different mechanisms, among them impairment of inhibitor accessibility to the NNIBP, modification of critical intermolecular interactions, or introduction of steric hindrance.^{2,5,6,9}

NNRTIs have evolved from the first inhibitors such as nevirapine to the imidoylthiourea (ITU) and subsequently to the more potent diaryltriazine (DATA) and diarylpurimidine (DAPY) analogues (Figure 1). First-generation inhibitors encompass voluminous and rigid structures, while DATA and DAPY inhibitors are similar in volume but possess a central ring joining two flexible lateral rings (wings I and II, Figure 1). Crystallographic studies show that nevirapine binds in a *butterfly*-like conformation,^{10,11} while ITU, most DATA, and DAPY inhibitors bind in a *horseshoe* conformation.^{7,12} The DAPYs have increased flexibility inside the binding site, involving a combination of rotational (*wiggling*) and translational (*jiggling*) shifts, and are very potent inhibitors against both wild-type and mutated RT.^{5,7,13,14}

In this work, we present a detailed analysis of the structure, molecular interactions in the binding pocket, energetics, and dynamics of drugs ranging from first- to third-generation compounds, bound to wtRT and K103N mutated RT (mRT). Starting structures are obtained from the reported crystallographic structures or predicted by means of molecular docking procedures. The solvated complexes are subject to molecular dynamics followed by free energy decomposition analyses, in search of a quantitative structure–activity model correlating the binding energetics to the reported anti-HIV activities (EC₅₀).

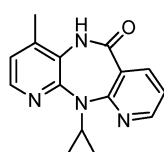
COMPUTATIONAL METHODS

Initial Structures of the Nonnucleoside Reverse Transcriptase Inhibitor–Reverse Transcriptase Complexes. The complexes of compounds **1**, **2**, **4**, **5**, **7**, and **9** with wtRT and those of compounds **1** and **8** with mRT were obtained

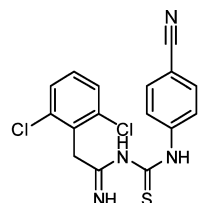
* Corresponding authors. E-mail: mmadrid@psc.edu (M.M.) or macribri@fcq.unc.edu.ar (M.C.B.).

[†] Universidad Nacional de Córdoba.

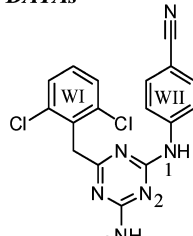
[‡] Pittsburgh Supercomputing Center.

a) First generations NNRTIs

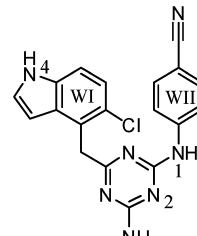
1. nevirapine



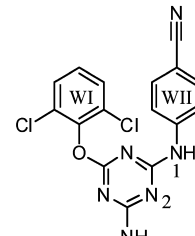
2. R100943 (ITU)

b) DATAs

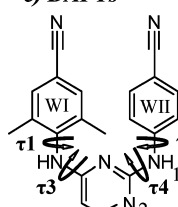
3. R106168



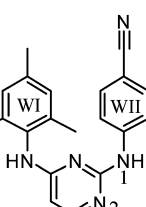
4. R120393



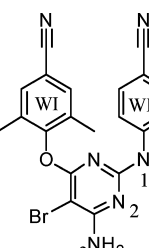
5. R129385

c) DAPYs

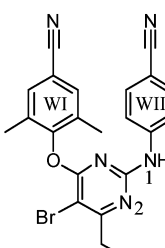
6. R152929



7. TMC120



8. TMC125



9. R185545

Figure 1. Chemical structures of the studied nonnucleoside RT inhibitors.

from the RCSB Protein Databank.¹⁵ PDB IDs are 1VRT,¹⁰ 1S6P,⁷ 1S9G,⁷ 1S9E,⁷ 1S6Q,⁷ 1SUQ,⁷ 1FKP,¹⁶ and 1SV5,⁷ respectively.

Molecular docking techniques were used to obtain the starting structures of those complexes whose crystallographic structures were not available at the time these studies were conducted. The crystallographic structure of wtRT with compound **9** (PDB ID 1SUQ)⁷ was used for the molecular docking of compounds **3**, **6**, and **8** in the binding site of

wtRT; and that of mRT with complex **8** (PDB ID 1SV5)⁷ was used for the other DAPYs to mRT. After these studies were completed, the crystallographic structure of compound **8** complexed to wtRT (PDB ID 3MEC) was reported.¹² We compare our docked structure to this crystallographic structure in the Results and Discussion section. To date, no crystallographic structures of DATAs complexed to mRT have been reported. Therefore, a reliable structure for the

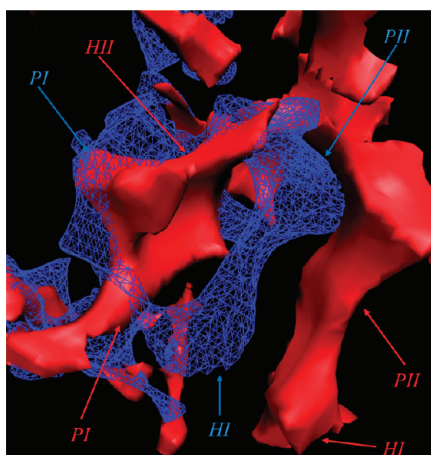
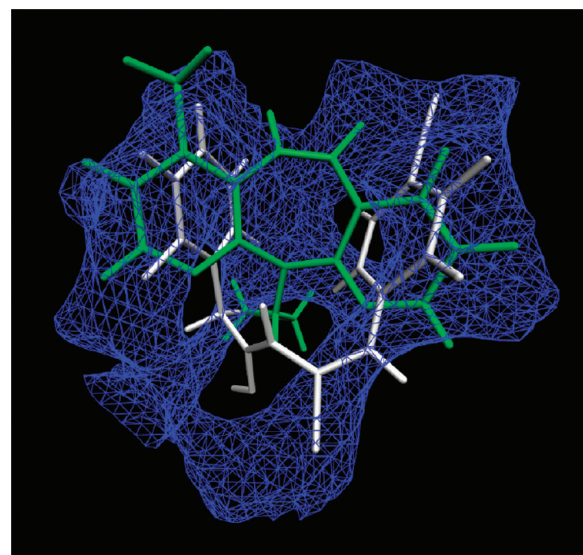
**Figure 2.** Topologies of the NNIBP of wtRT (blue wireframe) and mRT (red solid surface). PI is formed by Pro95, Tyr181, Tyr188, Gly190, Trp229, Leu234, and Thr107. PII is formed by Lys101, Val106, His235, Pro236, and Tyr318. HI is located near Lys101 and Glu138. HII is lined by Pro95, Thr107, and Val189.**Figure 3.** Binding mode of compounds **1** (green) and **2** (white) to the NNIBP of wtRT.

Table 1. Nonnucleoside Reverse Transcriptase Inhibitor Interactions in the Binding Pocket Compared to Their Potency against Wild-Type and K103N Mutated Reverse Transcriptase

compd	wtRT		mRT	
	EC ₅₀ ^a (μM)	binding pocket interactions ^b	EC ₅₀ ^a (μM)	binding pocket interactions ^b
1	0.0850	PI, PII	2.4670	PI, PII
2	0.0030	PI, PII, HI, H-bond Lys101		c
3	0.0020	PI, PII, HI, H-bond Lys101 and Glu138		c
4	0.0030	PI, PII, HI, H-bond Lys101		c
5	0.0030	PI, PII, HI, H-bond Lys101 and Glu138		c
6	0.0004	PI, PII, HI, H-bond Lys101	nd ^d	PI, PII, HI, H-bond Lys101 and Glu138
7	0.0010	PI, PII, HI, H-bond Lys101	0.0040	PI, PII, HI, H-bond Lys101 and Glu138, water-mediated
8	0.0020	PI, PII, HI, H-bond Lys101	0.0010	PI, PII, HI, H-bond Lys101 and Glu138, water-mediated
9	0.0040	PI, PII, HI, H-bond Lys101	0.0040	PI, PII, HI, H-bond Lys101 and Glu138

^a EC₅₀ is the half-maximal effective concentration.⁷ ^b PI is lined by Pro95, Tyr181, Tyr188, Gly190, Trp229, Leu234, and Thr107. PII is composed by Lys103, Val106, His235, Pro236, and Tyr318. HI is located near Lys101 and Glu138. ^c No structure available. ^d Not determined.

docking of DATAs to mRT is not available, and these dockings are not presented.

After addition of H-atoms, all complexes are solvated and subjected to energy minimization and molecular dynamics procedures.

Molecular Docking, Molecular Dynamics, and Free Energy Decomposition. Ligands are built by use of the Gabedit software,¹⁷ after which conformational searches are performed with Gaussian98,¹⁸ by application of the AM1 semiempirical method.¹⁹ The minimum energy conformation is further optimized at the ab initio (HF6-31G*) level, with the goal of obtaining a minimum energy conformation that allows a representative charge assignment over each atom. Restrained electrostatic potential (RESP) fitted charges are computed with Gaussian98.¹⁸ Atom parameters are added to the ff99 force field with the module *xLeap* of Amber8.²⁰

The complexes with wtRT and mRT are subject to energy minimization with the sander module of Amber8.²⁰ Affinity grids are constructed on the minimized structures by use of AutoGrid.²¹ Docking assays are carried out by use of the AutodockTools and Autodock3.²² The lowest-energy and most populated clusters of docked conformations are selected for the molecular dynamics (MD) simulations. Intermolecular interactions are visualized with *LigPlot*.²³

The complexes are solvated by use of a pre-equilibrated TIP3P water model, by application of a solvent box with a minimum distance from the solute of 8 Å in each direction. After minimization and equilibration, MDs are carried out at 300 K for 3 ns, with the *pmemd* module of Amber8.²⁰ Hydrogen bonds and dihedral angles are analyzed with the *ptraj* module of Amber8.²⁰ The trajectories are processed by VMD^{24,25} and Sirius programs.²⁶ The free energy of binding to the NNIBP is estimated by the molecular mechanics/Poisson–Boltzmann surface area (MM-PBSA) method,²⁷ integrated in Amber8.²⁰

$$G = E_{\text{MM}} + G_{\text{solv}} - T\Delta S \quad (1)$$

where *G* is the Gibbs free energy; *T* is the absolute temperature; ΔS is the entropic change; *E_{MM}* is the total molecular mechanic energy, which includes internal (bond, angle, dihedral), van der Waals, and electrostatic terms; and $G_{\text{solv}} = G_{\text{pol}} + G_{\text{np}}$, where *G_{pol}* is the electrostatic component of the solvation free energy, which was computed by the Poisson–Boltzmann approximation,²⁸ and *G_{np}* is the non-polar contribution to the solvation free energy, calculated

by an empirical model. The solvent was treated as a continuum model of high-dielectric ($\epsilon = 80$) and the solute as a low-dielectric medium ($\epsilon = 1$) with embedded charges.²⁹ Details of all aspects of the simulations are given in the Supporting Information.

RESULTS AND DISCUSSION

Topology of the Nonnucleoside Inhibitor Binding Pocket of Wild-Type and Mutated Reverse Transcriptase. Two main hydrophobic pockets oriented in a parallel position (PI and PII in Figure 2, blue) are identified from the nitrogen affinity grids of the NNIBP of wtRT (PDB ID 1SUQ).⁷ PI is lined by Pro95, Tyr181, Tyr188, Gly190, Trp229, Leu234, and Thr107, while PII is defined by Lys103, Val106, His235, Pro236, and Tyr318 (Figure S1, Supporting Information). Additionally, a hydrophilic region is observed in the lower portion of the NNIBP (HI in Figure 2, blue), located near Lys101 and Glu138 between PI and PII (Figure S2, Supporting Information).

The binding cavity of K103N mRT (PDB ID 1SV5)⁷ is more voluminous, with a larger distance between PI and PII (Figure 2, red). HI is significantly displaced with respect to wtRT, being now fused to PII. This NNIBP topology and larger volume can result in increased ligand accessibility to an upper hydrophilic region lined by Pro95, Thr107, and Val189 (HII in Figure 2, red).

Binding of Nonnucleoside Reverse Transcriptase Inhibitors to Reverse Transcriptases. *Nevirapine* and *Imidoylthiourea*. In the reported crystallographic structure of **1** with wtRT,¹⁰ the lateral aromatic rings are located inside PI and PII, respectively, and the central ring is positioned in the center of the binding site cavity [Figure 3 (green) and Figure S3, Supporting Information].

The complex between **1** and mRT is obtained from the reported crystallographic structure.¹⁶ When bound to mRT, compound **1** occupies more the most hydrophobic cavity in the NNIBP, the PI region, than the PII region (Figure S4, Supporting Information). This binding pattern results in the loss of interactions with PII and might be responsible for the reported 29-fold decrease in potency of compound **1** when bound to mRT⁷ (Table 1).

In the reported crystallographic structure of the complex of **2** with wtRT,⁷ wings I and II are located in PI and PII, respectively. In addition, the linker chain between wings I and II is positioned toward HI, with the 1-NH moiety

Table 2. Energetic Components and Biological Activity of Nonnucleoside Reverse Transcriptase Inhibitors Complexed to Wild-Type Reverse Transcriptase

compd	ELE ^a (kcal/mol)	vdW ^b (kcal/mol)	$\Delta G_{\text{nonpolar}}^c$ (kcal/mol)	$\Delta G_{\text{polar}}^d$ (kcal/mol)	ΔG_{tot}^e (kcal/mol)	−log EC ₅₀ ^f
1	−8.40 (±2.75)	−43.55 (±1.82)	−4.78 (±0.31)	23.52 (±2.47)	−33.21 (±1.96)	1.07
2	−17.98 (±3.17)	−48.56 (±2.37)	−5.37 (±0.36)	30.96 (±2.41)	−40.95 (±2.56)	2.52
3	−27.01 (±4.38)	−51.60 (±2.53)	−5.98 (±0.37)	35.70 (±3.44)	−48.90 (±2.92)	2.70
4	−13.31 (±3.14)	−50.65 (±3.00)	−5.88 (±0.32)	29.69 (±2.26)	−40.16 (±2.9)	2.52
5	−25.82 (±4.69)	−50.96 (±2.61)	−5.74 (±0.35)	32.40 (±3.8)	−50.12 (±2.48)	2.52
6	−18.13 (±3.44)	−54.03 (±2.28)	−6.11 (±0.35)	30.33 (±2.85)	−47.94 (±2.54)	3.40
7	−19.25 (±2.69)	−53.57 (±2.28)	−6.05 (±0.3)	29.44 (±2.04)	−49.42 (±2.59)	3.00
8	−19.79 (±6.73)	−49.55 (±3.95)	−6.48 (±0.29)	29.93 (±4.82)	−45.89 (±4.24)	2.70
9	−27.03 (±5.65)	−61.05 (±2.84)	−6.67 (±0.27)	40.35 (±4.46)	−54.39 (±2.67)	2.40

^a Electrostatic. ^b van der Waals. ^c Nonpolar contribution. ^d Polar contribution. ^e Total binding free energy. ^f Half-maximal effective concentration.⁷

Table 3. Energetic Components and Biological Activity of Nonnucleoside Reverse Transcriptase Inhibitors Complexed to Mutated Reverse Transcriptase

compd	ELE ^a (kcal/mol)	vdW ^b (kcal/mol)	$\Delta G_{\text{nonpolar}}^c$ (kcal/mol)	$\Delta G_{\text{polar}}^d$ (kcal/mol)	ΔG_{tot}^e (kcal/mol)	−log EC ₅₀ ^f
1	−1.49 (±3.46)	−40.71 (±2.39)	−4.87 (±0.27)	18.49 (±3.80)	−23.71 (±3.53)	−0.39
7	−4.57 (±2.35)	−45.98 (±2.37)	−6.20 (±0.39)	21.91 (±1.86)	−34.84 (±2.61)	2.40
8	−5.32 (±4.6)	−51.21 (±2.43)	−6.48 (±0.31)	24.79 (±4.02)	−38.21 (±2.57)	3.00
9	−30.20 (±4.15)	−56.55 (±2.97)	−7.04 (±0.33)	36.91 (±2.28)	−56.88 (±2.83)	2.40

^a Electrostatic. ^b van der Waals. ^c Nonpolar contribution. ^d Polar contribution. ^e Total binding free energy. ^f Half-maximal effective concentration.⁷

establishing hydrogen bonds with Lys101 [Figure 3 (white) and Figure S5, Supporting Information].

During the 3 ns molecular dynamics simulation, compound **1** does not form any direct or solvent water-mediated hydrogen bonds with residues of wtRT or mRT. In both complexes, compound **1** maintains its original position, where the main intermolecular interactions are hydrophobic contacts between **1** and residues lining PI and PII. During the MD simulations of **2** complexed to wtRT, a sustained hydrogen bond between the NH moiety of the central linker and the oxygen of the Lys101 backbone carbonyl is observed, with an occupancy of 82.9% of the overall trajectory. As expected, wings I and II establish hydrophobic interactions with several residues lining PI and PII.

The energetic components and the total free energy of interaction (ΔG_{tot}) for wtRT and mRT are calculated during the last nanosecond of simulation by applying the molecular mechanics/Poisson–Boltzmann surface area (MM-PBSA) approach (Tables 2 and 3, respectively). A significant increase in ΔG_{tot} is observed for the complex of **1** with mRT with respect to wtRT (−33.21 and −23.71 kcal/mol for wtRT and mRT, respectively). The K103N mutation in the binding pocket results in an increase in the electrostatic and van der Waals energies, in agreement with the marked loss in inhibitory activity against the mutated RT strain.

The ΔG_{tot} of compound **2** bound to wtRT is lower than that of compound **1**. This difference arises mainly from the electrostatic component. In fact, compound **2** establishes a sustained, direct hydrogen bond with Lys101. Since compound **2** is 28 times more active than **1** against wtRT,⁷ our findings suggest that the drugs' efficacy might be enhanced when electrostatic interactions are established with residues from HI together with hydrophobic contacts in PI and PII.

Dihydropyridine-triazine. To analyze the binding mode of the three DATA compounds to wtRT, docking procedures were performed for **3**, while the crystallographic structures were

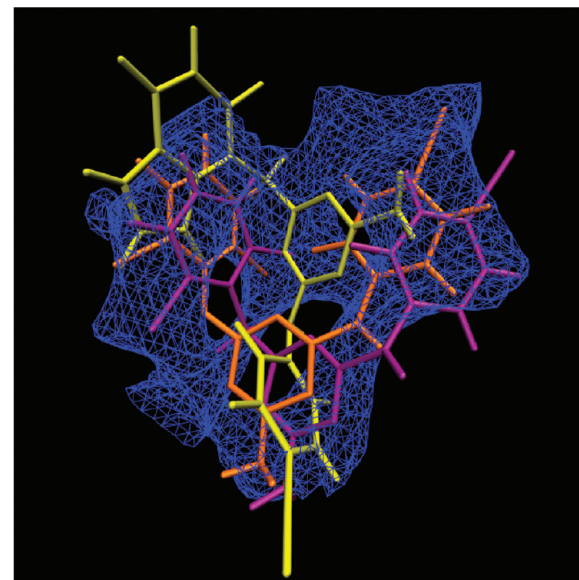


Figure 4. Binding mode of compounds **3** (purple), **4** (yellow), and **5** (orange) in the NNIBP of wtRT.

used for **4** and **5**.⁷ Homologous binding modes are observed for these three compounds with wtRT (Figure 4), with wing I oriented toward PI, wing II positioned in PII, the central ring occupying the core cavity of the NNIBP, and the 3-NH₂ amine located in HI (Figures S6 and S7, Supporting Information). In this conformation, intermolecular interactions are established with the three main NNIBP regions (PI, PII, and HI), which is consistent with the reported anti-HIV activity of these DATAs being comparable to that of compound **2** (Table 1).

Sustained hydrogen bonds between the ligand and the backbone carbonyl oxygen of Lys101 are identified during the MDs of the complexes of **3**, **4**, and **5** with wtRT. Compounds **3** and **5** interact with Lys101 through the 1-NH

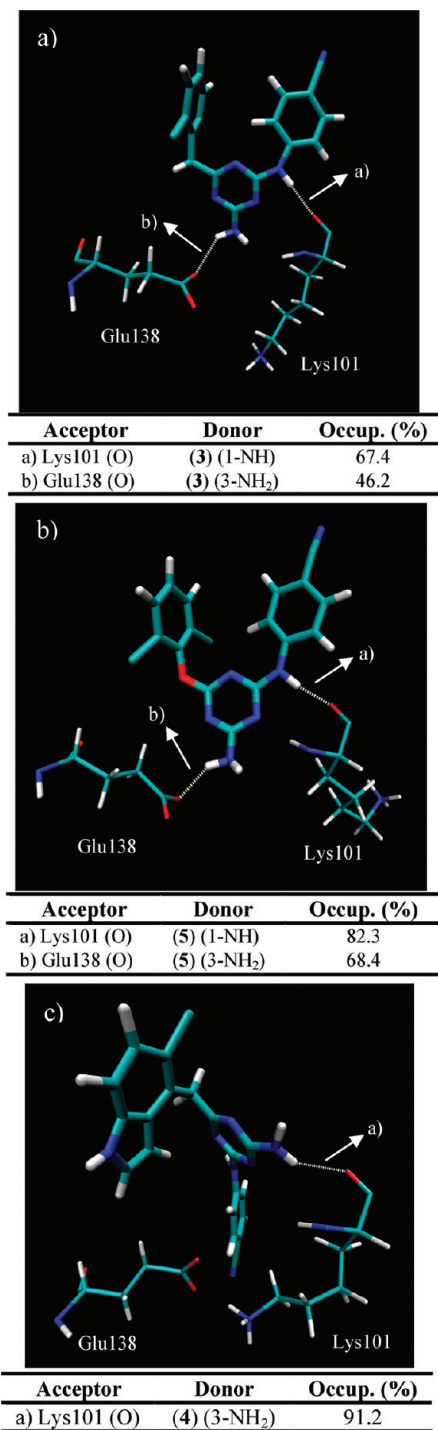


Figure 5. Hydrogen bonds between compounds (a) 3, (b) 5, and (c) 4 and residues of the NNIBP of wtRT.

moiety linking wing II with the central ring (Figure 5a,b) with occupancy of 67.4% and 82.3%, respectively. The primary amine in the central ring (3-NH₂) establishes a hydrogen bond with the side-chain carboxyl group of Glu138 (occupancy 46.2% and 68.4%, respectively) (Figure 5a,b). In contrast, compound 4 also establishes a sustained hydrogen bond with the Lys101 backbone carbonyl oxygen but involving the primary amine (3-NH₂) moiety (occupancy 91.2%) (Figure 5c).

The energetic analysis (Table 2) shows that compounds 3 and 5 have substantially lower ΔG_{tot} than compound 4. This lower ΔG_{tot} for compounds 3 and 5 originates mainly in the electrostatic component, since compounds 3 and 5 establish

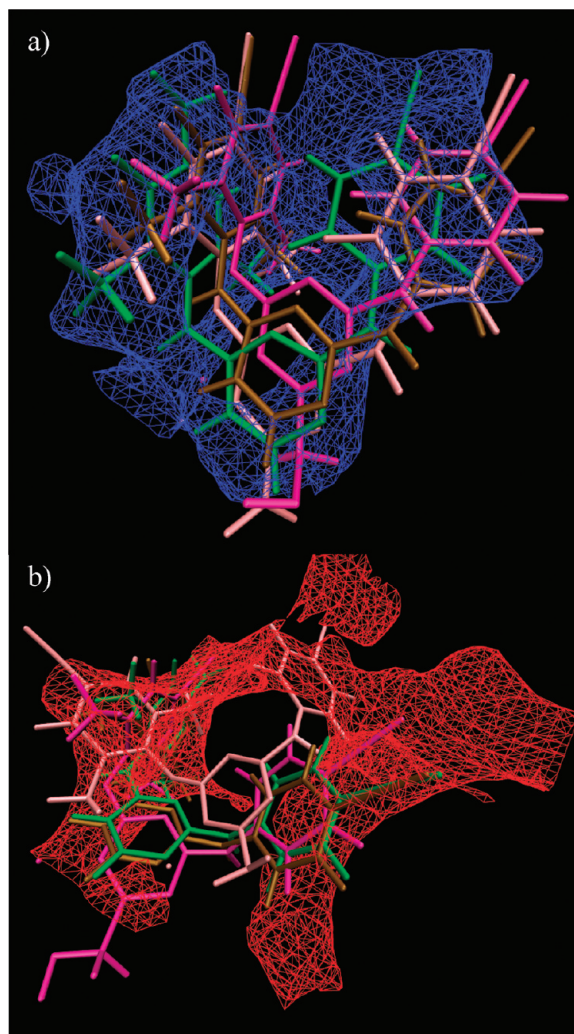


Figure 6. Binding mode of compounds 6 (brown), 7 (green), 8 (pink), and 9 (magenta) in the NNIBP of (a) wtRT and (b) mRT.

a hydrogen bond with Glu138 in addition to the one with Lys101. However, despite the difference in electrostatic interactions, compounds 4 and 5 have the same biological activity. These observations suggest that the electrostatic interaction with Glu138 does not affect the compound's biological activity against wtRT.

Dialylypyrimines. The docking of compounds 6 and 8 to wtRT shows that these compounds bind in a similar conformation to that of the crystallographic complexes of 7 and 9 with wtRT⁷ (Figure 6a and Figures S1 and S2, Supporting Information). We had completed the docking and molecular dynamics of compound 8 to wtRT when the crystallographic structure of this compound became available (PDB ID 3MEC).¹² The docked and crystallographic structures are very similar (Figure 7), validating the docking results for compound 8. Compound 8 establishes intermolecular interactions in PI, PII, and HI (Table 1).

The MD trajectories of 6–9 with wtRT show sustained hydrogen bonds between the 1-NH moiety linking the central ring of the DAPYs and the carbonyl oxygen of Lys101 (Figure 8), with occupancies of 92.4%, 85.4%, 91.8%, and 73.7%, respectively.

The complexes between 6, 7, and 9 with mRT are obtained by molecular docking procedures, while the MD simulations of 8 with mRT are started from its crystallographic structure

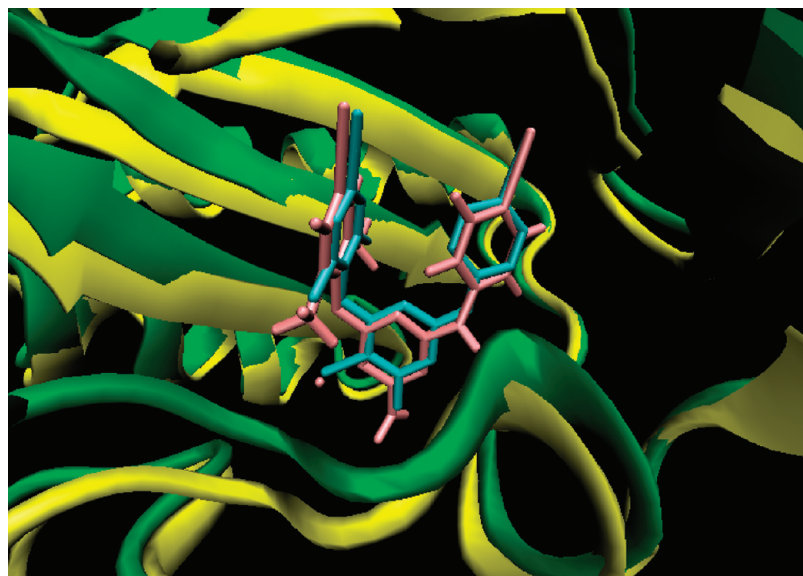


Figure 7. Superposition of the docked compound **8** (ligand in pink, NNIBP in green) and the crystallographic structure 3MEC (ligand in blue, NNIBP in yellow). The superposition is based on the alignment of the NNIBP C_α.

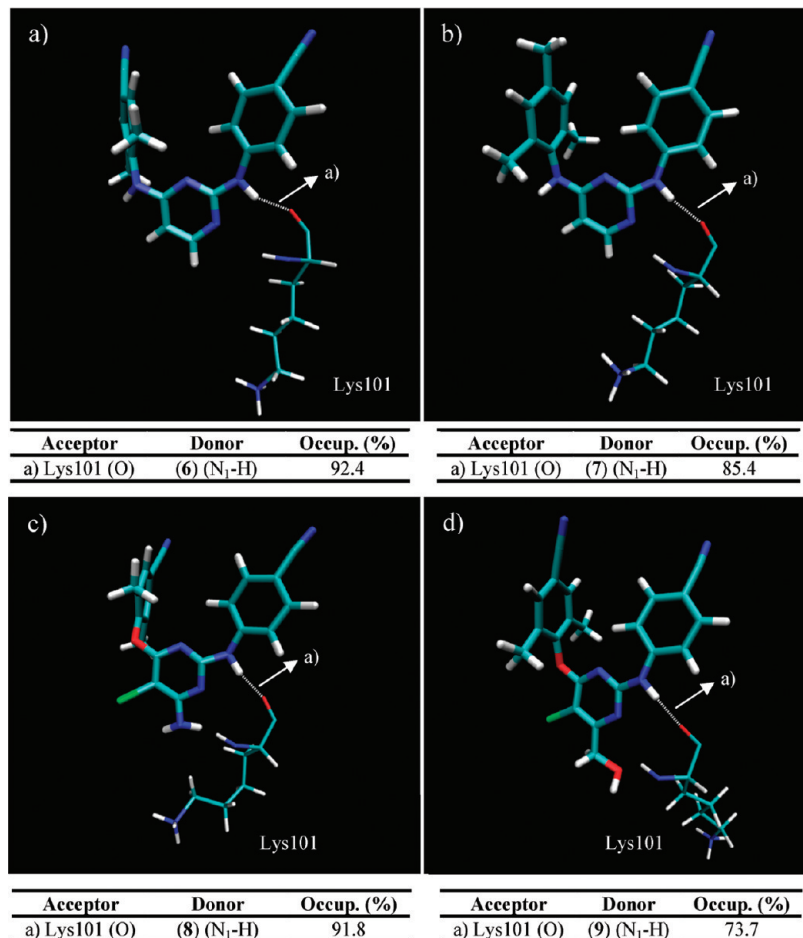


Figure 8. Hydrogen bonds between compounds (a) **6**, (b) **7**, (c) **8**, and (d) **9** and residues in the NNIBP of wtRT.

(Figure 6b and Figure S9, Supporting Information).⁷ During the MD simulations with mRT, all these compounds adopt the usual *horseshoe* conformation, establishing sustained hydrogen bonds with Lys101 and Glu138 in HI (Figure 9).

Compounds **7** and **8** with mRT establish water-mediated hydrogen bonds with Lys101 and Glu138 (Figure 9a,b), which, when the high mobility of solvent molecules is considered, are expected to be energetically highly optimized.

The hydroxymethyl substitution in the central ring of compound **9** displaces the water molecule involved in the bonding network observed in **7** and **8**. Compound **9** therefore forms direct hydrogen bonds with Lys101 and Glu138 through its 1-NH (73% occupancy) and OH (98% occupancy) moieties, respectively (Figure 9c).

The antiviral potencies of complexes **7** and **8** against mRT are closely related to their van der Waals energetic compo-

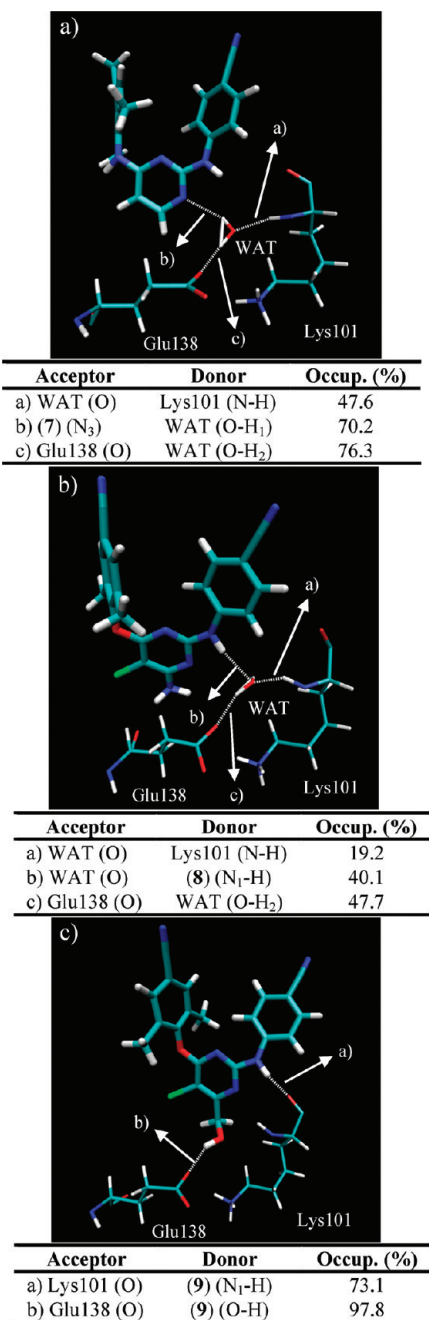


Figure 9. Hydrogen bonds between compounds (a) 7, (b) 8, and (c) 9 and residues in the NNIBP of mRT.

nents. Compound 7 exhibits a 4-fold decrease in its activity compared to that of wtRT due to an increase in the van der Waals energy (-53.57 and -45.98 kcal/mol for wtRT and mRT, respectively). In contrast, compound 8 exhibits a decrease in the van der Waals energy compared to that of wtRT (-49.55 and -51.21 kcal/mol for wtRT and mRT, respectively), which is in agreement with the 2-fold increase in potency.

The electrostatic components for 7 and 8 are considerably smaller than any of the other simulated DATA and DAPY molecules (Table 3). The main electrostatic interactions between these DAPY compounds and mRT are water-mediated hydrogen bonds. These interactions are not taken into account in the MM-PBSA method, due to the use of an implicit solvent environment, thus underestimating the electrostatic interactions for these compounds. In contrast,

compound 9 establishes non-water-mediated hydrogen bonds and exhibits a significantly stronger electrostatic component.

Conformational Analyses. In order to analyze the positions of wings I and II with respect to the central ring of compounds 3–8, the dihedral angles (defined in Figure 1) of the DATA and DAPY compounds are studied during the MD trajectories of wtRT and mRT (Table 4).

The values adopted by τ_1 and τ_3 show that, for the majority of the compounds analyzed, wing I is in a perpendicular position slightly to the back with respect to the central ring, maximizing the $\pi-\pi$ stacking interactions with Tyr181, Tyr188, and Trp229 in PI. Substitutions that favor this arrangement may enhance antiviral activity. A classic strategy would encompass the introduction of an additional fused ring to restrain τ_1 values around 90° , but this would also diminish the drug's flexibility, which has been identified as a critical property to enhance antiviral potency.^{5,7} Substituents in the ortho position of wing I favor this spatial arrangement due to steric hindrance, without restraining the ligand flexibility. In fact, it has been found that DATA and DAPY compounds with chlorine and methyl moieties, respectively, on wing I are more active against wtRT and mRT than their unsubstituted counterparts.⁵

The large standard deviations of τ_2 indicate that wing II undergoes large rotations during the trajectories. Despite this, the compounds can still maintain hydrophobic interactions with the residues in PII, because these interactions do not require a defined spatial arrangement. In fact, PII lacks aromatic residues capable of establishing $\pi-\pi$ stacking interactions, which are strongly based on a coplanar alignment. Substituents on the ortho position of wing II might diminish antiviral activity due to a reduction in ligand flexibility and mobility. In fact, the most potent DATA and DAPYs do not incorporate substituents in positions 2 or 6 of wing II, which would hinder τ_2 rotations.

The angles τ_2 , τ_3 , and τ_4 of compound 8 (TMC125) undergo large variations during the trajectory. These results are consistent with the difficulties reported for crystallizing TMC125-wtRT.⁷

Relation between Energetic Components and Antiviral Potency. There is a strong correlation between the van der Waals energetic component determined by MM-PBSA and the reported antiviral activity against wtRT (eq 2, Figure 10). The correlation suggests that higher potencies are expected for those compounds that establish hydrophobic contacts in PI and PII and is in agreement with the high hydrophobicity of the NNIBP of wtRT.

$$\begin{aligned} -\log EC_{50-wtRT} &= -0.194(\pm 0.026)vDW - 7.200(\pm 1.305) \\ r &= 0.950 \quad r^2 = 0.903 \quad SD = 0.226 \quad F = 56.04 \quad n = 8 \end{aligned} \quad (2)$$

The only outlier to this correlation is compound 9. Both lateral wings of compound 9 are deeply buried into the PI and PII pockets of the binding site (Figure S2, Supporting Information), resulting in a higher van der Waals component than those of the other compounds studied, but this is not accompanied by a higher antiviral activity.

CONCLUSIONS

We apply molecular docking and molecular dynamics techniques to study the binding interactions, flexibility, and free energies of binding of several NNRTIs complexed to

Table 4. Average Dihedral Angles and Their Standard Deviations during the 3 ns MD Trajectories

compd	dihedral angle (avg \pm SD, deg)							
	τ_1		τ_2		τ_3		τ_4	
	wtRT	mRT	wtRT	mRT	wtRT	mRT	wtRT	mRT
3	-85 \pm 9	nd	11 \pm 30	nd	-34 \pm 21	nd	6 \pm 17	nd
4	-64 \pm 9	nd	11 \pm 14	nd	-55 \pm 12	nd	42 \pm 16	nd
5	-90 \pm 11	nd	18 \pm 20	nd	-28 \pm 14	nd	-4 \pm 14	nd
7	-96 \pm 9	93 \pm 13	15 \pm 14	-34 \pm 15	-28 \pm 13	6 \pm 14	4 \pm 13	2 \pm 14
8	-82 \pm 12	-82 \pm 12	2 \pm 32	-4 \pm 31	-9 \pm 35	-2 \pm 32	-7 \pm 22	-4 \pm 21
9	-83 \pm 10	86 \pm 10	23 \pm 17	10 \pm 17	-16 \pm 12	-13 \pm 12	-7 \pm 14	-22 \pm 14

wtRT and K103N mRT, and we correlate these properties to their reported biological activities.

The docked compounds [R106168 (**3**), R129385 (**5**), TMC125 (**8**) with wtRT, and R152929 (**6**), TMC120 (**7**) and R185545 (**9**) with mRT] bind in similar positions and establish similar interactions as those reported in the crystallographic structures of other DATA and DAPY compounds. We find that all ITU, DATA, and DAPY compounds studied establish hydrogen bonds with Lys101, which are sustained during the 3 ns molecular dynamics simulations of both wtRT and mtRT. The complexes of R106168 (**3**) and R129385 (**5**) with wtRT form also a hydrogen bond with Glu138. However, the existence of this additional hydrogen bond does not correlate with a higher biological activity against wtRT. Indeed, we find that the biological activity of all complexes (except compound **9**) varies linearly with the van der Waals energetic component when bound to wtRT, providing a predictive tool for the design of effective inhibitors against wtRT.

The presence of the K103N mutation results in a more voluminous NNIBP and modifies its electrostatic properties. The four DAPY complexes studied with mRT form hydrogen bonds with Lys101 and Glu138. In the case of TMC120 (**7**) and TMC125 (**8**), these electrostatic interactions are water-mediated. In particular, two water molecules are observed during the trajectory forming a hydrogen-bond network between Lys101, Glu138, and TMC125 (**8**). Thus, RT inhibitors with activity against both wild-type and K103N mutated HIV strains not only establish hydrophobic interactions with the NNIBP, which have been vastly described for first-generation NNRTIs, but also attain specific intermo-

lecular interactions with a hydrophilic region in the lower part of the binding pocket (located near Lys101 and Glu138).

According to the correlation observed in this work, a potent inhibitor of wtRT must maximize its van der Waals interactions in the binding pocket. In addition, it is known that the drugs' flexibility is essential for the drugs to be also effective against mutations.⁷ During the MD trajectories, wing I of the DATA and DAPY compounds remains at $\sim 90^\circ$, while wing II undergoes large rotations in the hydrophobic cavity formed by Lys103, Val106, His235, Pro236, and Tyr318. This observation is in agreement with the conclusions that these compounds are able to accommodate themselves in the binding pocket so as to remain bound and effective in the presence of RT mutations.⁷ These conclusions provide a valuable tool for the rational design of effective inhibitors with better therapeutic profiles for the treatment of AIDS.

ACKNOWLEDGMENT

We gratefully acknowledge financial support from the Secretaría de Ciencia y Técnica of the Universidad Nacional de Córdoba (SECYT-UNC), the Consejo Nacional de Investigaciones Científicas y Técnicas (CONICET), and the Agencia Nacional de Promoción Científica y Tecnológica (FONCyT) of Argentina. This research was supported in part by the National Science Foundation through TeraGrid resources provided by the Pittsburgh Supercomputing Center (TG-MCB070070N). S.R.R. also acknowledges fellowships from CONICET.

Supporting Information Available: Nine figures showing two-dimensional intermolecular interaction and ligand position of complexes between NNRTIs and residues in the NNIPB of wtRT and mRT; details of the computational method; and full citations for refs 7, 13, 18, and 20. This material is available free of charge via the Internet at <http://pubs.acs.org>.

REFERENCES AND NOTES

- (1) De Clercq, E. Highlights in the development of new antiviral agents. *Mini Rev. Med. Chem.* **2002**, 2, 163–175.
- (2) Sarafianos, S. G.; Marchand, B.; Das, K.; Himmel, D. M.; Parniak, M. A.; Hughes, S. H.; Arnold, E. Structure and function of HIV-1 reverse transcriptase: Molecular mechanisms of polymerization and inhibition. *J. Mol. Biol.* **2009**, 385, 693–713.
- (3) Prajapati, D. G.; Ramajayam, R.; Yadav, M. R.; Giridhar, R. The search for potent, small molecule NNRTIs: A review. *Bioorg. Med. Chem.* **2009**, 17, 5744–5762.
- (4) Cohen, J. Therapies. Raising the limits. *Science* **2002**, 296, 2322.
- (5) Das, K.; Lewi, P. J.; Hughes, S. H.; Arnold, E. Crystallography and the design of anti-AIDS drugs: conformational flexibility and positional adaptability are important in the design of non-nucleoside HIV-1 reverse transcriptase inhibitors. *Prog. Biophys. Mol. Biol.* **2005**, 88, 209–231.

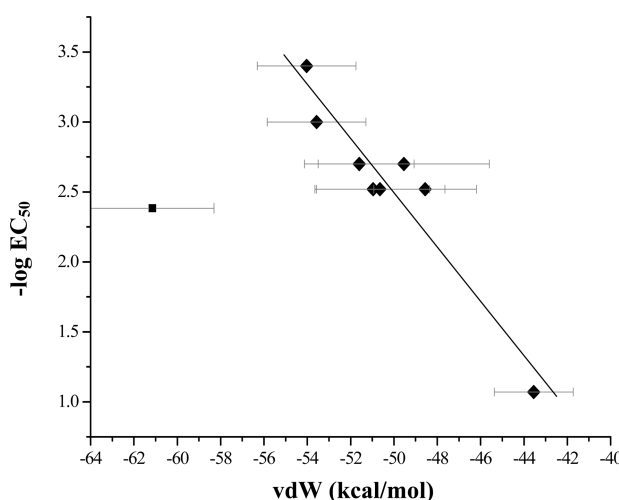


Figure 10. Biological activity ($-\log EC_{50}$) vs van der Waals energetic component for wtRT.

- (6) Hsiou, Y.; Ding, J.; Das, K.; Clark, A. D., Jr.; Boyer, P. L.; Lewi, P.; Janssen, P. A.; Kleim, J. P.; Rosner, M.; Hughes, S. H.; Arnold, E. The Lys103Asn mutation of HIV-1 RT: a novel mechanism of drug resistance. *J. Mol. Biol.* **2001**, *309*, 437–445.
- (7) Das, K.; et al. Roles of conformational and positional adaptability in structure-based design of TMC125-R165355 (etravirine) and related non-nucleoside reverse transcriptase inhibitors that are highly potent and effective against wild-type and drug resistant HIV-1 variants. *J. Med. Chem.* **2004**, *47*, 2550–2560.
- (8) Ragni, R.; Frasca, S.; Manetti, F.; Brizzi, A.; Massa, S. HIV-reverse transcriptase inhibition: Inclusion of ligand-induced fit by cross-docking studies. *J. Med. Chem.* **2005**, *48*, 200–212.
- (9) Ren, J.; Nichols, C. E.; Stamp, A.; Chamberlain, P. P.; Ferris, R.; Weaver, K. L.; Short, S. A.; Stammers, D. K. Structural insights into mechanisms of non-nucleoside drug resistance for HIV-1 reverse transcriptases mutated at codons 101 or 138. *FEBS J.* **2006**, *273*, 3850–3860.
- (10) Ren, J.; Esnouf, R.; Garman, E.; Somers, D.; Ross, C.; Kirby, I.; Keeling, J.; Darby, G.; Jones, Y.; Stuart, D. High resolution structures of HIV-1 RT from four RT-inhibitor complexes. *Nat. Struct. Biol.* **1995**, *2*, 293–302.
- (11) Ding, J.; Das, K.; Moereels, H.; Koymans, L.; Andries, K. Structure of HIV-1 RT/TIBO R 86183 complex reveals similarity in the binding of diverse nonnucleoside inhibitors. *Nat. Struct. Biol.* **1995**, *2*, 407–415.
- (12) Lansdon, E. B.; Brendza, K. M.; Hung, M.; Wang, R.; Mukund, S.; Jin, D.; Birkus, G.; Kutty, N.; Liu, X. Crystal structure of HIV-1 reverse transcriptase with etravirine (TMC125) and rilpivirine (TMC278): Implications for drug design. *J. Med. Chem.* **2010**, *53*, 4295–4299.
- (13) Janssen, P. A. J.; et al. In search of a novel anti-HIV drug: Multidisciplinary coordination in the discovery of 4-[[4-[(1E)-2-cyanoethenyl]-2,6-dimethylphenyl]amino]-2-pyrimidinyl]amino]benzonitrile (R278474, rilpivirine). *J. Med. Chem.* **2005**, *48*, 1901–1909.
- (14) Van Herrewege, Y.; Vanham, G.; Michiels, J.; Fransen, K.; Kestens, L.; Andries, K.; Janssen, P. A. J.; Lewi, P. A series of diaryltriazines and diarylpyrimidines are highly potent nonnucleoside reverse transcriptase inhibitors with possible applications as microbicides. *Antimicrob. Agents Chemother.* **2004**, *48*, 3684–3689.
- (15) Berman, H. M.; Westbrook, J.; Feng, Z.; Gilliland, G.; Bhat, T. N.; Weissig, H.; Shindyalov, I. N.; Bourne, P. E. The Protein Data Bank. *Nucleic Acids Res.* **2000**, *28*, 235–242.
- (16) Ren, J.; Milton, J.; Weaver, K. L.; Short, S. A.; Stuart, D. I.; Stammers, D. K. Structural basis for the resilience of efavirenz (DMP-266) to drug resistance mutations in HIV-1 reverse transcriptase. *Struct. Fold. Des.* **2000**, *8*, 1089–1094.
- (17) Allouche, A. R. Gabedit - A graphical user interface for computational chemistry softwares. *J. Comp. Chem.* **2011**, *32*, 174–182.
- (18) Frisch, M. J.; et al. Gaussian 98; Gaussian Inc., Pittsburgh, PA, 1998.
- (19) Dewar, M. J. S.; Zoebisch, E. G.; Healy, E. F.; Stewart, J. J. P. AM1: a new general purpose quantum mechanical molecular model. *J. Am. Chem. Soc.* **1985**, *107*, 3902–3909.
- (20) Case, D. A.; et al. AMBER8; University of California, San Francisco, CA, 2004.
- (21) Morris, G. M.; Goodsell, D. S.; Halliday, S.; Huey, R.; Hart, W. E.; Belew, R.; Olson, A. J. Automated docking using a Lamarckian genetic algorithm and an empirical binding free energy function. *J. Comput. Chem.* **1998**, *19*, 1639–1662.
- (22) Morris, G. M.; Goodsell, D. S.; Huey, R.; Hart, W. E.; Halliday, S.; Belew, R.; Olson, A. J. Autodock3; Molecular Graphics Laboratory, Department of Molecular Biology, The Scripps Research Institute, La Jolla, CA, 1999.
- (23) Wallace, A. C.; Laskowski, R. A.; Thornton, J. M. LIGPLOT: A program to generate schematic diagrams of protein–ligand interactions. *Protein Eng.* **1995**, *8*, 127–134.
- (24) Humphrey, W.; Dalke, A.; Schulten, K. VMD: Visual molecular dynamics. *J. Mol. Graphics* **1996**, *14*, 33–38.
- (25) Eargle, J.; Wright, D.; Luthey-Schulten, Z. Multiple alignment of protein structures and sequences for VMD. *Bioinformatics* **2006**, *22*, 504–506.
- (26) Sirius software v.1.2; San Diego Supercomputer Center, University of California, San Diego, California, 2008.
- (27) Kuhn, B.; Gerber, P.; Schulz-Gasch, T.; Stahl, M. Validation and use of the MM-PBSA approach for drug discovery. *J. Med. Chem.* **2005**, *48*, 4040–4048.
- (28) Sharp, K. A.; Honing, B. Electrostatic interactions in macromolecules: theory and applications. *Annu. Rev. Biophys. Biophys. Chem.* **1990**, *19*, 301–332.
- (29) Cornell, W. D.; Cieplak, P.; Bayly, C. I.; Gould, I. R.; Merz, K. M.; Ferguson, D. M.; Spellmeyer, D. C.; Fox, T.; Caldwell, J. W.; Kollman, P. A. A second generation force field for the simulation of proteins, nucleic acids, and organic molecules. *J. Am. Chem. Soc.* **1995**, *117*, 5179–5197.

CI1001636